

BULETINUL INSTITUTULUI POLITEHNIC DIN IAȘI  
Publicat de  
Universitatea Tehnică „Gheorghe Asachi” din Iași  
Volumul 62 (66), Numărul 3, 2016  
Secția  
MATEMATICĂ. MECANICĂ TEORETICĂ. FIZICĂ

## IMPEDANCE CHARACTERIZATION OF A DEEP BRAIN STIMULATING ELECTRODE: AC ELECTROCHEMICAL IMPEDANCE SPECTROSCOPY

BY

BOGDAN NEAGU<sup>1</sup> and EUGEN NEAGU<sup>2,3,\*</sup>

<sup>1</sup>Toronto Western Research Institute, University Health Network and Division of Neurology,  
Department of Medicine, University of Toronto, Toronto, Canada

<sup>2</sup>Universidade Nova de Lisboa, Caparica, Portugal,  
Departamento de Ciência dos Materiais

<sup>3</sup>“Gheorghe Asachi” Technical University of Iași,  
Department of Physics

Received: November 18, 2016

Accepted for publication: December 16, 2016

**Abstract.** The impedance of the Medtronic 3387 deep brain stimulation (DBS) electrode was characterized using electrochemical impedance spectroscopy (EIS). The interface meta-saline was modeled as a parallel combination of faradaic resistance ( $R_F(f,j)$ ) and double layer capacitance ( $C_{dl}(f,j)$ ). The model took in consideration the dependence of  $R_F(f,j)$  and  $C_{dl}(f,j)$  of frequency  $f$  and current density  $j$ . The coupling capacitance between the metallic wires was included in the model.  $C_{dl}(f,j)$  and  $R_F(f,j)$  were determined from the fit of the data to the electrical model. We documented a significant frequency-dependent voltage drop on the interface and it influences the spread of the stimulation voltage. The electrical efficiency of the electrode was small for low frequencies, increased to 56% at 3 kHz and was constant for higher frequencies.

**Keywords:** metal-saline interface; impedance spectroscopy; deep brain stimulation.

---

\*Corresponding author; *e-mail*: euneagu1@yahoo.com

## 1. Introduction

The Medtronic 3387 DBS electrode (Medtronic® Inc, Minneapolis, MN, USA) is used in therapy (stimulation) or electrophysiological recordings. Constant voltage (voltage-controlled) stimulation imposes a voltage spread within the brain that depends on the impedances of the contact-electrolyte interface and of the tissue (Butson and McIntyre, 2005; Miocinovic *et al.*, 2009). The frequency and  $j$  dependence of the impedance of the contact-electrolyte interface can be monitored with EIS (Macdonald, 1992; Cogan, 2008). Few studies report on the interface impedance behavior for  $j$  above the linearity limit (Ragheb and Geddes, 1990; Schwan and Maczuk, 1965; Geddes *et al.*, 1971). The impedance was measured *in vitro* (Holsheimer *et al.*, 2000; Wei and Grill, 2009) or *in vivo* (Wei and Grill, 2009) using biphasic constant-voltage pulses (Holsheimer *et al.*, 2000), biphasic square current pulses and sinusoidal signals of 1 Hz to 10 kHz (Wei and Grill, 2009). EIS measurements were carried on a scaled-down version of the DBS electrode, suitable for implantation in the non-human primate brain (Lempka *et al.*, 2009).

A detailed description of the electrical impedance of the Medtronic 3387 DBS electrode and the contact-saline interface with stimulation settings relevant for therapy is currently lacking. This is because the design of the DBS electrode is complex from the electrical impedance measurements point of view. Also it has been difficult to determine the interface impedance from the measurements because the saline impedance (bulk impedance) was approximated with the asymptotic high frequency impedance (Holsheimer *et al.*, 2000; Wei and Grill, 2009). Overlooking the impedance of the contact-electrolyte interface can affect the volume of neuronal activation (McIntyre *et al.*, 2004), the tendency for tissue damage (McCreery *et al.*, 1990) and electrode corrosion (Shepherd and Clark, 1991).

Previous electrical models of the Medtronic 3387 DBS electrode neglected the coupling capacitance between the leads (Holsheimer *et al.*, 2000; Wei and Grill, 2009). An accurate description of the electrode impedance and of the contact-saline interface impedance will further our knowledge in several directions: understand the relation between the stimulation voltage and the current passing through tissue *in vivo*, establish a relation between the stimulation voltage and the voltage actually delivered to the tissue, analysis of the *in vivo* EIS data and for the development of computational models of neural recording and stimulation.

The goal of this study was to propose a quantitative electrical model for the DBS electrode impedance and the contact-saline interface. The model accounts for the nonlinear dependence of  $R_F(f,j)$  and  $C_{al}(f,j)$  with frequency and current density. Our results complete the previous published work on DBS electrode.

## 2. Methods

Broad-band EIS was performed for two adjacent contacts of the Medtronic 3387 DBS electrode (the electrode has four platinum iridium contacts, Fig. 1).

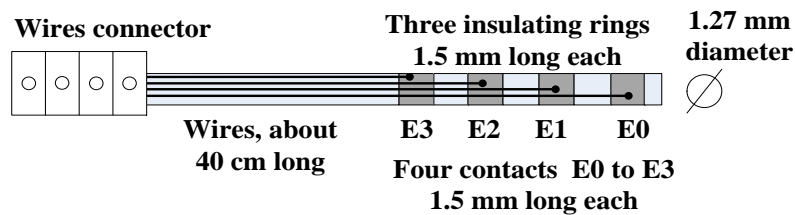


Fig. 1 – The Medtronic 3387 electrode for deep brain stimulation.

### 2.1. Electrochemical Impedance Spectroscopy

Sine wave signal was used to measure the impedance using a QuadTech 7600 Precision Resistance-Capacitance-Inductance meter. The range of stimulation frequencies was 10 Hz to 2 MHz with 106 frequency points, 20 points for a frequency decade, spaced logarithmically. We used constant current (0.3 to 6 mA rms;  $j$  from 5 to 100 mA cm<sup>-2</sup>) and voltage-controlled stimulation signals (0.3 to 1 V, rms). If not otherwise noted, the reported results are for 1 V rms voltage-controlled sinusoidal signal or for 1 mA rms constant current. These values are relevant for therapeutic stimulation settings. Measurements were performed in a tank filled with 2 l saline, placed in a Faraday cage. Measurements were carried in different saline concentrations for two reasons: i) the electrical conductivity of the tissue can be lower than that of 0.9% saline; ii) to detect the variation of  $C_{dl}(f,j)$  and  $R_f(f,j)$  with saline conductivity. At the same time an encapsulation layer may form on the surface of the electrode which is equivalent to a decrease of the electrical conductivity of the medium. Unless otherwise noted, the saline was 0.154 M NaCl (9 g/l, conductivity 1.5 S m<sup>-1</sup>). In addition to measurements in saline, the impedance was measured: with the DBS electrode in the air to measure the coupling capacitance between the leads ( $C_{le}$ ), including the individual contacts of the DBS electrode, and the electrical resistance ( $R_l$ ) of the 2x40 cm long leads; with the DBS electrode in distilled water to estimate the capacitance between two adjacent contacts ( $C_{cl}$ ). If not otherwise noted, the measurements were replicated three times at identical conditions and the mean values are presented.

## 2.2. Electrical Model of the DBS Electrode

### 2.2.1. Electrode in the Air

The impedance of the leads running from the DBS electrode connectors to the contacts,  $Z_l(f)$ , has real and imaginary components. The real component ( $R_l$ ) is determined by the length of the metallic leads between the DBS electrode connectors and the contacts and by the resistance of the insulating material around the metallic leads  $R_d$ . The imaginary component of  $Z_l(f)$  has three parts: (i) the coupling capacitance  $C_{le}$  between the metallic leads running from the DBS electrode connector to the contacts, (ii) the inductance of the leads which is small and was neglected and (iii) the capacitance  $C_{cl}$  between the two adjacent contacts.  $R_d$  is important during measurements with the electrode in the air. The equivalent circuit of the DBS electrode in the air is shown in Fig. 2a.

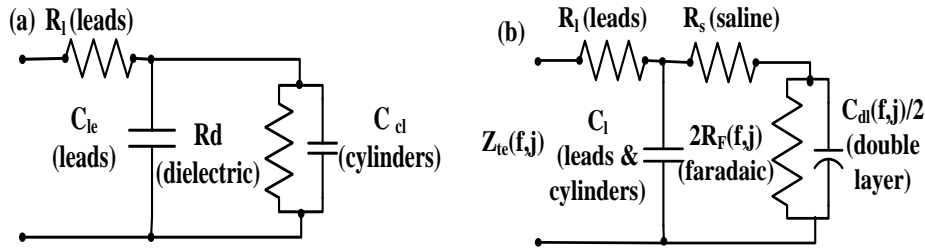


Fig. 2 – a) The equivalent circuits of the DBS electrode in air for the case of bipolar configuration; b) The equivalent circuits of the DBS electrode in saline solution for the case of bipolar configuration.

### 2.2.2. Electrode in Saline

We made the following assumptions: (i)  $R_d$  was negligible, thus  $C_{le}$  and  $C_{cl}$  appeared connected in parallel and they were replaced by  $C_l$ ; (ii) the two electrode–saline interfaces have the same impedance characteristics.

$R_s$  was in series with the interface impedance  $Z_{dl}(f,j)$  which consisted of an  $f$  and  $j$  dependent double layer capacitance  $C_{dl}(f,j)/2$  in parallel with an  $f$  and  $j$  dependent faradaic resistance  $2R_F(f,j)$ . The equivalent circuit of the DBS electrode in saline is shown in Fig. 2b. The parallel equivalent circuit of the electrode consists of  $R_p(f,j)$  in parallel with  $C_p(f,j)$ . The impedance of the DBS electrode measured in saline was  $Z(f,j)$ . The theoretical impedance (components showed in Fig. 2b) was  $Z_{te}(f,j)$ . To determine  $C_{dl}(f,j)$  and  $R_F(f,j)$  we need an analytical equation for  $Z_{te}(f,j)$ . We assumed that:

$$C_{dl}(f, j) = \frac{C_{dl0}(j)}{f^n} \quad (1)$$

and:

$$R_F(f, j) = \frac{R_{F0}(j)}{f^m} \quad (2)$$

where  $C_{dl0}(j)$  (units  $\text{Fs}^{-n}$ ) was a measure of the double layer capacitance at 1 Hz,  $n$  was a measure of the deviation from pure capacitive behavior,  $R_{F0}(j)$  (units  $\Omega\text{s}^{-m}$ ) was a measure of the faradaic resistance at 1 Hz and  $m$  was a measure of the deviation from pure ohmic behavior.

### 3. Results

#### 3.1. Resistance of the Lead Wires

With the electrode in the air and contacts E1 and E2 short-circuited,  $R_l$  was  $86.4 \pm 0.3 \Omega$  (5 measurements), comparable with previous results (Holsheimer *et al.*, 2000; Wei and Grill, 2009).

#### 3.2. Electrode Impedance

The measured  $C_p(f)$  and  $R_p(f)$  of the electrode in air, distilled water or saline (0.4, 2 and 9 g/l) are shown in Fig. 3 for 1V rms. Similar results were reported by measurements in buffered saline solution with frequencies in the range 1 Hz to 10 kHz (Wei and Grill, 2009).

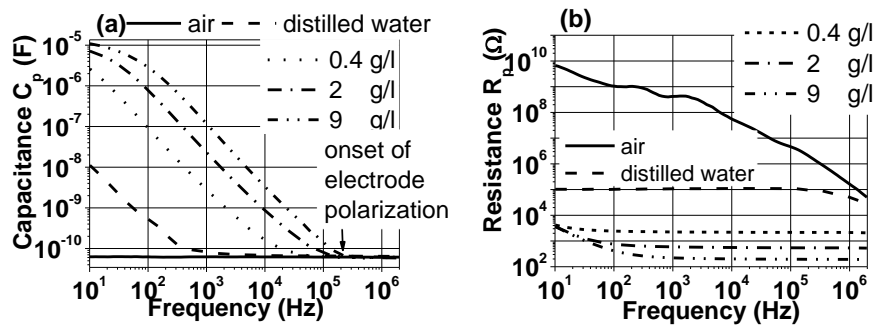


Fig. 3 – *a*) The equivalent parallel capacitance  $C_p(f)$  of the DBS electrode. The arrow indicates the onset of electrode polarization. The onset frequency is lower as the saline concentration is lower; *b*) The equivalent parallel resistance  $R_p(f)$  of the DBS electrode. Above a certain frequency which increases with saline concentration  $R_p$  is frequency-independent and allows to calculate the geometry factor.

Clinical measurements of the DBS electrode impedance reported values between 415 and 1999  $\Omega$  (Coffey, 2008). These values are higher than the

values reported in Fig. 3b for 0.9% NaCl concentration. Data in Fig. 3b allows to calculate the geometry factor (GF) as 0.0058 m for bipolar configuration and 0.0049 m for monopolar configuration. The electrode capacitance increased with decreasing frequency due to the ion charges accumulating at the metal-saline interface (Bard and Faulkner, 1980; Ackmann and Seitz, 1984; McAdams and Jossinet, 1995). The onset of electrode polarization was clearly observed (Fig. 4a) while complete electrode polarization (the frequencies for which the capacitance was constant) was not. The capacitance of the Medtronic DBS electrode was estimated to be 3.3  $\mu\text{F}$  (Butson and McIntyre, 2005) or 1.5  $\mu\text{F}$  (Holsheimer *et al.*, 2009). Our results showed that 3.3  $\mu\text{F}$  was the capacitance at 112 Hz in 0.9% saline. The equivalent resistance  $R_p(f)$  increased at low frequencies and the increase was higher for higher NaCl concentration. The capacitive or resistive nature of the current depends on the frequency and the conductivity of the solution. This is why we tested a large range of saline concentrations. The main contribution to  $C_p(f)$  was given by the double layer capacitance, yet  $C_p(f)$  does not represent the double layer capacitance. The double layer capacitance and the faradaic resistance will be obtained by fitting the data to the analytical model we presented.

### 3.3. Impedance Dependence on Current Density

Because the double layer impedance changes with  $j$  (Bard and Faulkner, 1980; Lempka *et al.*, 2009; Schwan, 1968), the electrode impedance changes with  $j$ . Fig. 4 shows the measured impedance  $|Z_t(f,j)|$  and  $C_p(f,j)$  with the DBS electrode in physiologic saline for 0.3, 1 and 6 mA. The impedance decreased when the current increased. The dependence of the impedance with  $j$  decreased when  $f$  increased. For frequencies higher than 3 kHz the impedance was independent of  $j$ . Fig. 4b showed that for low frequencies the capacitance increased with  $j$ . For frequencies higher than 300 Hz, the capacitance did not depend on  $j$ . For frequencies higher than 3 kHz, the resistance was independent of  $j$  (data not shown).

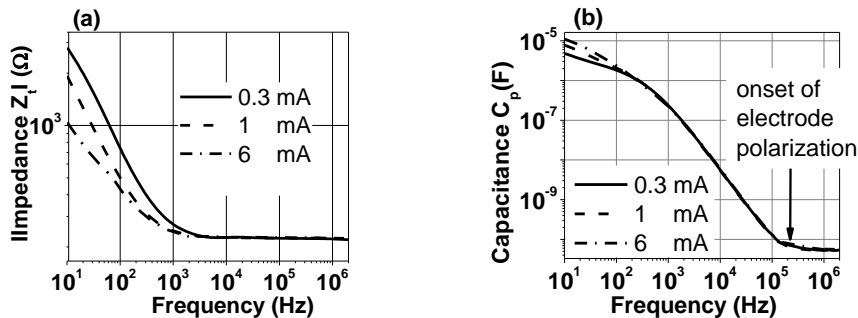


Fig. 4 – a) The impedance modulus  $|Z_t(f,j)|$  measured with the DBS electrode in physiologic saline for three values of the current: 0.3, 1 and 6 mA (current density 5 to 100  $\text{mA cm}^{-2}$ ); b) The equivalent parallel capacitance  $C_p(f,j)$  of the DBS electrode measured in the same conditions as above.

### 3.4. Monopolar Configuration

We measured the impedance when a stimulation voltage of 1 V was applied between E1 and an AgCl reference electrode. The results in Fig. 5 show that the impedance was smaller for monopolar configuration. The monopolar and bipolar impedances decreased with increasing  $f$  and above 3 kHz the decrease was insignificant.

### 3.5. The Coupling Capacitance Between the Leads and the Geometrical Capacitance Between Two Adjacent Contacts

The capacitance was constant ( $6.20 \times 10^{-11}$  F, Fig. 3a) between 10 Hz and 2 MHz when the DBS electrode was in the air. The total impedance of the electrode in the air is characteristic for capacitive impedance:

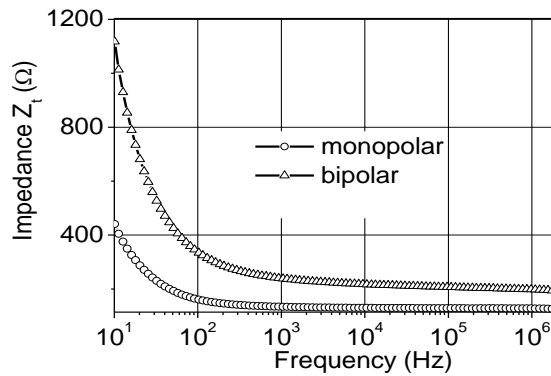


Fig. 5 – The absolute value of the impedance of the DBS electrode in 0.9% NaCl saline for the case of monopolar (circles) and bipolar (triangles) configuration. The applied voltage was 1V rms.

$$X_c = \frac{1}{\omega C_l} \quad (3)$$

where  $\omega = 2\pi f$  is the angular frequency. Eq. (3) was used to fit the data from Fig. 3a and determine  $C_l$ . The capacitance in the air was  $C_l = C_{le} + C_{cl} = (6.21 \pm 0.08) \times 10^{-11}$  F, similar to the result from Fig. 3a.

The real part of the dielectric permittivity of pure water is constant ( $\epsilon' = 78$ ) for frequencies from 0 Hz to several GHz. Fig. 3a shows that for  $f > 10$  kHz the capacitance was frequency independent with a value of  $6.44 \times 10^{-11}$  F. The capacitance of the contacts was estimated from the difference between the high-frequency capacitances (MHz range) in air and distilled water. The value was  $C_{cl} = (3.1 \pm 0.9) \times 10^{-14}$  F. The capacitance of the two cylinders is very small compared to the coupling capacitance.

This conclusion is important for the use of electrode for EIS *in vivo*. The signal recorded *in vivo* depends on the capacitance of the contacts and the phenomena that take place at the metal-tissue interface. If the geometrical capacitance of the contacts is small, the recorded signal is small. This can result in a small Signal/Noise ratio, thus affecting data analysis.

### 3.6. Calculation of the Double Layer Capacitance and the Faradaic Resistance

For saline concentrations above 0.4%, the resistance decreased with increasing  $f$  and the variation was higher for higher NaCl concentrations (Fig. 3b). Above 1 kHz, the resistance was almost  $f$  independent and it is thought to reflect the saline resistance (Holsheimer *et al.*, 2000; Wei and Grill, 2009). The measured resistance has 2 components:  $R_l$  and  $R_s$ .

We used a fitting procedure (and the theoretical model) to determine the unknown parameters:  $C_{dl0}(j)$ ,  $n$ ,  $R_{F0}(j)$  and  $m$ . The circles in Fig. 6a represent  $Z_t(f)$  for 0.9% NaCl and 6 mA and the solid line is the best fit curve. The circles in Fig. 6b represent  $C_p(f)$  for 0.9% NaCl and 6 mA and the solid line is the best fit curve.

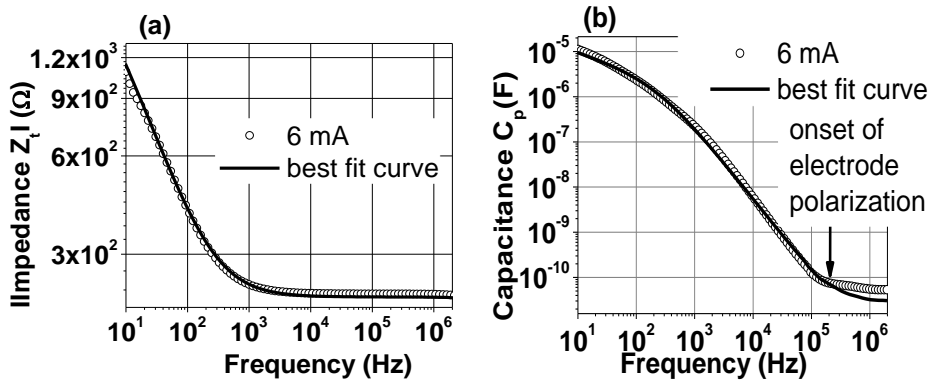


Fig. 6 – Typical fitting curves to determine the unknown parameters  $C_{dl0}(j)$ ,  $n$ ,  $R_{F0}(j)$  and  $m$ .

The fit for  $C_p(f)$  is less precise for  $f > 0.3$  MHz. This may happen because at high  $f$  the coupling capacitance between the leads is the main capacitance and it is distributed along the leads. The data obtained for  $n$  and  $m$  are weakly but linearly dependent on logarithm of  $j$ .  $C_{dl0}$  and  $R_{F0}$  cannot be expressed as simple functions of  $j$ . When  $j$  decreases,  $C_{dl0}$  and  $n$  decrease and  $R_{F0}$  and  $m$  increase.  $C_{dl0}$  and  $n$  are less sensitive to  $j$  than  $R_{F0}$  and  $m$ .  $R_s$  was calculated using the geometry factor GF.

**Table 1**

The Values of  $C_{dl0}$ ,  $n$ ,  $R_{F0}$  and  $m$  obtained from the Fitting of the Experimental Data for Different  $j$  with the Proposed Model. The Relative Errors Affecting the Parameters are Below 7% for  $C_{dl0}$  and  $R_{F0}$  and Below 4% for  $n$ ,  $m$

$j$ , [mA cm <sup>-2</sup> ]	$C_{dl0}$ , [Fs <sup>-n</sup> ]	$n$	$R_{F0}$ , [ $\Omega$ s <sup>-m</sup> ]	$m$
100	62.11 x10 <sup>-6</sup>	0.360	5088	0.259
66.7	44.81 x10 <sup>-6</sup>	0.341	8570	0.291
33.3	37.11 x10 <sup>-6</sup>	0.309	14226	0.350
16.7	29.21 x10 <sup>-6</sup>	0.291	22167	0.401
11.7	22.11 x10 <sup>-6</sup>	0.272	34265	0.439
5	14.41 x10 <sup>-6</sup>	0.250	55453	0.490

The data in Table 1 are in good agreement with the general behavior of  $C_{dl}$  and  $R_F$  at different current densities above the linearity limit (Ragheb and Geddes, 1990; Onaral and Schwan, 1983). Because the  $f$  range was large and the number of the unknown parameters deduced from the fitting procedure was low, the fitting procedure yielded unique values for the parameters. We know all the components of the equivalent circuit presented in Fig. 2b.

#### 4. Discussion

Our goal was to provide an electrical model for DBS electrode impedance and to characterize the contact-saline impedance which is part of a complex electrical circuit. We made distinction between the saline solution, the metal-saline interface and other components related to DBS electrode design.

##### 4.1. Model of the Equivalent Electric Circuit for the Interface Impedance

Previous studies modeled the DBS electrode interface with  $f$  independent lumped components (Holsheimer *et al.*, 2000), constant phase element (Lempka *et al.*, 2009) or an  $f$  and  $j$  dependent resistor in parallel with an  $f$  and  $j$  dependent capacitor (Wei and Grill, 2009). We make here a step further and show how  $C_{dl}(f,j)$  and  $R_F(f,j)$  change with  $f$  and  $j$  for therapy-relevant parameters. Eqs. (1) and (2) were used to quantify this variation (Onaral and Schwan, 1982; Geddes, 1997).

##### 4.2. Electrical Efficiency of the DBS Electrode

We propose to use the ratio between the voltage drop on the saline and the stimulation voltage to characterize the electrical (energy) efficiency of the electrode during the stimulation process. The voltage  $U_{ap}$  generated by the stimulator will determine a current:

$$I(f) = \frac{U_{ap}}{|Z_t(f)|} \quad (4)$$

The voltage drop on saline is:

$$U_s(f) = I(f)R_s \quad (5)$$

The electrical efficiency  $\eta(f)$  for a given current is:

$$\eta(f) = \frac{U_s(f)}{U_{ap}} = \frac{R_s}{|Z_t(f)|} \quad (6)$$

It reflects how much of the applied voltage will spread in the tissue and eventually contribute to stimulation. Eq. (6) is equally valid for constant current stimulation. Fig. 7 shows the electrical efficiency for three values of the current from 0.3 to 6 mA. The electrical efficiency was  $f$  dependent: it was low at low  $f$ , increased to 56% at 3 kHz and was constant at higher frequencies. For monopolar stimulation, when the implanted pulse generator is used as reference, the electrical impedance between the active contact and the reference was estimated at  $1001 \Omega$  (Walckiers *et al.*, 2010). The smallest value of the resistance for the stimulated volume can be approximated with  $R_s$  yet the electrical efficiency of monopolar stimulation is low. The efficiency will drop further if other series resistances at the electrode-tissue interface are taken into account such as the encapsulation layer at the surface of the contact or the implanted pulse generator. Finding solutions to decrease  $R_t$  seems reasonable in order to increase the electrical efficiency of the DBS electrode.

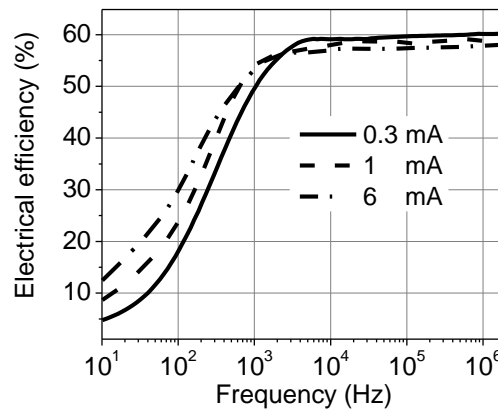


Fig. 7 – The electrical efficiency  $\eta(f)$  for three values of the current. The electrical efficiency is frequency dependent.

### 4.3. Electric Charge Transfer at the Interface

The capacitive current determines a capacitive charge transfer ( $Q_c(f)$ ) through the double layer capacitance and the resistive current determines a resistive charge transfer ( $Q_F(f)$ ) through the faradaic resistance.  $Q_c/Q_F$  can be used to evaluate the tendency of the stimulation process to cause electrode or tissue damage. Using the proposed model, for a given current the above ratio can be written as:

$$\frac{Q_c(f)}{Q_F(f)} = \frac{I_c(f)}{I_F(f)} = \omega R_F C_{dl} = 2\pi R_{F0} C_{dl0} f^{1-m-n} \quad (7)$$

Data in Table 1 show that  $m+n < 1$ . For the whole data range in Table 1  $Q_c/Q_F > 4$ , is  $j$  dependent and the ratio increases when  $f$  increase. The ratio  $Q_c/Q_F$  was relatively insensitive to frequency for  $f < 10$  kHz (Wei and Grill, 2009). When  $C_{dl}$  and  $R_F$  were calculated the coupling capacitance between the leads was neglected and the saline impedance was taken equal with the asymptotic high frequency impedance of the DBS electrode (Wei and Grill, 2009).

### 4.4. Limitations

Our results showed that the DBS electrode impedance was selectively parameter-dependent. The electrical models are complex and the complexity varies based on parameters variability. A major difficulty in choosing a model is the interface impedance whose  $f$  dependence is different from that of a capacitor. Although there are many attempts to model the metal-saline interface, we hereby propose a new model. Results from a large range of experimental conditions can be analyzed with this model. The model must be further completed if it were to describe the electrode behavior for lower frequencies of stimulation (below 10 Hz). It is known that the interface is nonlinear at low frequencies. In this situation the analysis of the higher order harmonic response of a system to sinusoidal current or voltage perturbation is useful (Richardot and McAdams, 2002). For frequencies higher than 0.6 MHz, the DBS electrode cannot be used for tissue electrical properties measurements because of the coupling capacitance between the leads.

We did not take into consideration the spatial variation of the current density along the contact (Bard and Faulkner, 1980). The model can be further refined if it includes the effects related to the presence of an encapsulation layer.

### 4.5. Clinical Relevance of the Results

The electrode is used for therapy, but its use for electrophysiological characterization of the nervous tissue presents a particular interest. The current

passing through tissue for a stimulation voltage can be calculated accurately if the electrode impedance is known. This may facilitate a better selection of the stimulation parameters. The average value of the impedance determined in patients is about 1200  $\Omega$  (range: 415–1999  $\Omega$ ) (Coffey, 2008). As a safety feature, the programming device calculates the charge density based on a conservative impedance value of 500  $\Omega$ . Our results showed that when the current varied from 0.3 to 6 mA the impedance varied between 600 and 400  $\Omega$ , when  $f$  varied from 50 to 300 Hz (Fig. 4a). For frequencies above 300 Hz the impedance was lower than 400  $\Omega$ . The clinical pulse repetition frequency range is between 130 and 185 Hz at pulse widths between 60 and 210  $\mu\text{s}$ . This results in harmonics above 2.38 kHz and for this frequency range our results showed that the parameter of interest for stimulation programming,  $Z_t(f,j)$  was practically  $j$  independent and  $f$  independent. The impedance was below the safety conservative impedance value and the electrode efficiency was about 56%. For a pulse duration of 200  $\mu\text{s}$  the fundamental harmonic is 2.5 kHz. Data in Table 1 shows that the relaxation time at this  $f$  is 2.5 ms. If pulse repetition frequency is 185 Hz ( $T = 5.4$  ms) the time between two pulses is too short for double layer capacitor discharging. Consequently charge balanced pulses (Coffey, 2008) are used to assure completely discharge of the double layer capacitor.

The ratio between the capacitive and resistive charge can be calculated using Eq. (7) and data in Table 1 and can be used to evaluate the tendency of the stimulation process to cause electrode or tissue damage.

We evaluate here the coupling capacitance between the leads and the geometrical capacitance between two adjacent contacts. They are important in understanding the upper  $f$  limit for electrode use to EIS measurements *in vivo*.

## 5. Conclusions

We proposed a model for the DBS electrode and contact-saline interface which accounts for the nonlinear dependence of  $R_F(f,j)$  and  $C_{dl}(f,j)$  with  $f$  and  $j$ . The impedance of the DBS electrode decreased when the applied voltage increased. The voltage dependence became less important with increasing frequency. For frequencies higher than 3 kHz the impedance was independent of the applied voltage (0.3 – 1 V rms) or  $j$  (5 to 100 mA  $\text{cm}^{-2}$ ), and it was below the safety conservative impedance value. The electrical (energy) efficiency of stimulation was  $f$  dependent and about 56% above 3 kHz for bipolar stimulation and lower for monopolar stimulation. The relaxation time of charge accumulated at the interface is 0.8 to 100 times the signal period indicating that the relaxation of the charge accumulated in the double layer is a slow process.

The geometrical capacitance of the active part of the DBS electrode was very low compared with the coupling capacitances  $C_{le}$  between the metallic wires. Consequently, a change of the dielectric properties of the medium around the electrode will determine a weak change of the collected signal.

## REFERENCES

- Ackmann J.J., Seitz A.S., *Methods of Complex Impedance Measurements in Biological Tissue*, CRC Crit. Rev. Biom. Eng., **10**, 281-311 (1984).
- Bard A.J., Faulkner L.R., *Electrochemical Methods: Fundamentals and Applications*, New York, Wiley, 1980.
- Butson C.R., McIntyre C.C., *Tissue and Electrode Capacitance Reduce Neural Activation Volumes During Deep Brain Stimulation*, Clin. Neurophysiol., **116**, 2490-500 (2005).
- Coffey R.J., *Deep Brain Stimulation Devices: A Brief Technical History and Review*, Artificial Organs, **33**, 208-220 (2008).
- Cogan S.F., *Neural Stimulation and Recording Electrodes*, Annu. Rev. Biomed. Eng., **10**, 275-309 (2008).
- Geddes L.A., *Historical Evolution of Circuit Models for the Electrode-Electrolyte Interface*, Ann. Biomed. Eng., **25**, 1-14 (1997).
- Geddes L.A., DaCosta C.P., Wise G., *The Impedance of Stainless-Steel Electrodes*, Med. & Biol. Eng., **9**, 511-521 (1971).
- Holsheimer J., Dijkstra E.A., Demeulemeester H., Nuttin B., *Chronaxie Calculated from Current-Duration and Voltage-Duration Data*, J. Neurosci. Method, **97**, 45-50 (2009).
- Lempka S., Miocinovic S., Johnson M.D., Vitek J.L., McIntyre C.C., *In Vivo Impedance Spectroscopy of Deep Brain Stimulation Electrodes*, J. Neural Eng., **6**, 321-332 (2009).
- McAdams E.T., Jossinet J., *Tissue Impedance—a Historical Overview*, Physiol. Meas., **16**, A1-3 (1995).
- McCreery D.B., Agnew W.F., Yuen T.G., Bullara L., *Charge Density and Charge per Phase as Cofactors in Neural Injury Induced by Electrical Stimulation*, IEEE Trans. Biomed. Eng., **37**, 996-1001 (1990).
- Macdonald J.R., *Impedance Spectroscopy*, Ann. Biomed. Eng., **20**, 289-305 (1992).
- McIntyre C.C., Mori S., Sherman D.L., Thakor N.V., Vitek J.L., *Electric Field and Stimulating Influence Generated by Deep Brain Stimulation of the Subthalamic Nucleus*, Clin. Neurophysiol., **115**, 589-595 (2004).
- Miocinovic S., Lempka S.F., Russo G.S., Maks C.B., Butson C.R., Sakaie K.E., Vitek J.L., McIntyre C.C., *Experimental and Theoretical Characterization of the Voltage Distribution Generated by Deep Brain Stimulation*, Exp. Neurol., **216**, 166-176 (2009).
- Onaral B., Schwan H.P., *Linear and Nonlinear Properties of Platinum Electrode Polarization, Part I: Frequency Dependence at Very Low Frequencies*, Med. Biol. Eng. Comput., **20**, 299-305 (1982).
- Onaral B., Schwan H.P., *Linear and Nonlinear Properties of Platinum Electrode Polarization. Part 2: A Time Domain Analysis*, Med. Biol. Eng. Comput., **21**, 210-216 (1983).
- Ragheb T., Geddes L.A., *Electrical Properties of Metallic Electrodes*, Med. Biol. Eng. Comput., **28**, 182-186 (1990).
- Richardot A., McAdams E.T., *Harmonic Analysis of Low-Frequency Bioelectrode Behavior*, IEEE Trans. Biomed. Imaging, **21**, 604-613 (2002).

- Schwan H.P., Maczuk J.G., *Electrode Polarization Impedance: Limits of Linearity*, Proc. 18th Ann. Conf. Eng., In Med. & Biol., 1965.
- Schwan H.P., *Electrode Polarization Impedance and Measurements in Biological Materials*, Ann. NY Acad. Sci., **148**, 191-209 (1968).
- Shepherd R.K., Clark G.M., *Scanning Electron Microscopy of Platinum Scala Tympani Electrodes Following Chronic Stimulation in Patients*, Biomaterials, **12**, 417-423 (1991).
- Walckiers G., Fuchs B., Thiran J.P., Mosig J.R., Pollo C., *Influence of the Implanted Pulse Generator as Reference Electrode in Finite Element Model of Monopolar Deep Brain Stimulation*, J. Neurosci. Methods, **186**, 90-96 (2010).
- Wei X.F., Grill W.M., *Impedance Characteristics of Deep Brain Stimulation Electrodes in Vitro and in Vivo*, J. Neural Eng., **6**, 4, 046008 (2009).

CARACTERIZAREA IMPEDANȚEI ELECTRODULUI PENTRU STIMULARE  
PROFUNDĂ ÎN CREIER: SPECTROSCOPIE  
DE IMPEDANȚĂ ELECTROCHIMICĂ ÎN CURENT ALTERNATIV

(Rezumat)

Impedanța electrodului pentru stimulare profundă în creier (DBS) Medtronic 3387 este caracterizată folosind spectroscopia de impedanță electrochimică (EIS). Interfața metal-soluție salină a fost modelată ca un circuit paralel format din rezistența  $R_F(f,j)$  și capacitatea stratului dublu  $C_{dl}(f,j)$ . Modelul ia în considerare dependența lui  $R_F(f,j)$  și  $C_{dl}(f,j)$  de frecvența  $f$  și densitatea de curent  $j$ . În model a fost inclusă și capacitatea parazită dintre firele metalice care fac legătura între cilindri și conector.  $C_{dl}(f,j)$  și  $R_F(f,j)$  au fost determinate din fitarea modelului teoretic cu datele experimentale. Se arată că există o importantă cădere de tensiune la interfață care afectează distribuția tensiunii de stimulare în creier. Randamentul electric al electrodului este mic pentru frecvențe joase, crește la 56% la 3 kHz și rămâne constant la frecvențe mai mari.